Research Article | Vol. 11, No. 7 / 1 July 2020 / Biomedical Optics Express 3659

Biomedical Optics EXPRESS

Optical coherence tomography and fluorescence microscopy dual-modality imaging for in vivo single-cell tracking with nanowire lasers

XUZHOU LI,[1,2,4] WEI ZHANG,[1,4] WILLIAM Y. WANG,[1] XIAOQIN WU,[1] YANXIU LI,[3] XIAOTIAN TAN,[1] DANIEL L. MATERA,[1] BRENDON M. BAKER,[1] YANNIS M. PAULUS,[1,3,5] XUDONG FAN,[1,6] AND XUEDING WANG[1,7]

[1]*Department of Biomedical Engineering, University of Michigan, 1101 Beal Ave., Ann Arbor, MI 48109, USA*
[2]*Department of Mechanical Engineering, University of Michigan, 2350 Hayward St., Ann Arbor, MI 48109, USA*
[3]*Department of Ophthalmology and Visual Sciences, University of Michigan, 1000 Wall St, Ann Arbor, MI 48105, USA*
[4]*Xuzhou Li and Wei Zhang contributed equally to this work*
[5]*ypaulus@med.umich.edu*
[6]*xsfan@umich.edu*
[7]*xdwang@umich.edu*

Abstract: Emerging cell-based therapies such as stem cell therapy and immunotherapy have attracted broad attention in both biological research and clinical practice. However, a long-standing technical gap of cell-based therapies is the difficulty of directly assessing treatment efficacy via tracking therapeutically administered cells. Therefore, imaging techniques to follow the *in vivo* distribution and migration of cells are greatly needed. Optical coherence tomography (OCT) is a clinically available imaging technology with ultrahigh-resolution and excellent imaging depth. It also shows great potential for *in vivo* cellular imaging. However, due to the homogeneity of current OCT cell labeling contrast agents (such as gold and polymer nanoparticles), only the distribution of entire cell populations can be observed. Precise tracking of the trajectory of individual single cells is not possible with such conventional contrast agents. Microlasers may provide a route to track unique cell identifiers given their small size, high emission intensities, rich emission spectra, and narrow linewidths. Here, we demonstrate that nanowire lasers internalized by cells provide both OCT and fluorescence signal. In addition, cells can be individually identified by the unique lasing emission spectra of the nanowires that they carry. Furthermore, single cell migration trajectories can be monitored both *in vitro* and *in vivo* with OCT and fluorescence microscopy dual-modality imaging system. Our study demonstrates the feasibility of nanowire lasers combined with the dual-modality imaging system for *in vivo* single cell tracking with a high spatial resolution and identity verification, an approach with great utility for stem cell and immunomodulatory therapies.

1. Introduction

Emerging cell-based therapies such as stem cell therapy and immunotherapy have drawn wide attention as novel therapeutics in medical research and clinical practice [1–4]. To evaluate the efficacy of the treatment, the determination of *in vivo* cell distribution, migration, and development is highly desired. However, the current assessment of therapeutics is mostly based on indirect methods [5,6], such as evaluating the efficiency of treatment by the size change of the

#395369 https://doi.org/10.1364/BOE.395369
Journal © 2020 Received 16 Apr 2020; revised 2 Jun 2020; accepted 3 Jun 2020; published 9 Jun 2020

Biomedical Optics EXPRESS

tumor or the anatomic recovery of the impaired area. There is still no technology that can directly monitor the distribution and migration of individual living cells *in vivo* over a long timescale which is especially important for understanding the mechanisms and improving the efficacy of cell-based therapies [7].

Optical coherence tomography (OCT) is a clinically available imaging technology with ultrahigh-resolution and excellent imaging depth [8–12]. This technology also has great potential for *in vivo* cellular imaging studies, especially for cell dynamic research [13–15]. Due to the minimal difference in optical scattering between cells and surrounding tissue layers, the original OCT imaging contrast of cell dynamics is poor. Therefore, contrast agents such as gold nanoparticles [16–20] and polymer microspheres [21] with strong scattering properties that can be internalized by targeted cells have been employed to improve imaging visibility. However, in most scenarios, both the contrast agent distribution and their optical properties in labeled cells are homogenous. Consequently, current OCT systems are only capable of observing the overall change in the distribution of the entire cell population [22]. Precise tracking of individual cells remains technically challenging with those conventional contrast agents.

Fluorescence labeling is a widely used technique to differentiate biological targets and monitor cell migration [23–26]. Multi-spectral fluorescence labels were also explored along with the intensity-based grayscale OCT imaging to provide distinguishable information to simultaneously track different cell groups [26]. However, as a result of the broad emission spectra of fluorophores, the number of different labels involved in multi-spectral fluorescence imaging is limited [23,26]. Geometrically encoded fluorescent DNA barcodes utilized the positions of the fluorophores on a DNA nanorod to provide over 200 distinct labels [24]. However, due to the sophisticated environment in tissue, the submicron resolution in fluorescent barcodes is significantly deteriorated. Therefore, it is difficult to employ this technique for *in vivo* studies.

In contrast, laser emission-based imaging has recently emerged as a novel technology in biomedical research. Notably, the microlasers have shown to be promising intracellular labels due to their small sizes, high emission intensities, rich emission spectra, and narrow linewidths [27–34]. It has been shown that those microlasers can be internalized by cells to either detect microenvironmental changes inside cells [30,33] or track individual cells [28,32]. Nonetheless, when imaged solely by fluorescence microscopy (FM), the cells containing microlasers can only be mapped by 2D images, while 3D information, albeit critical to locating the spatial positions of cells in biological tissues *in vivo*, is lost.

In this study, we developed an integrated OCT and FM dual-modality cell tracking system utilizing cadmium sulfide (CdS) nanowire lasers to track the 3D migration of individual cells *in vivo*. In this dual-modality system, the lasing spectra provide unique identity information for individual cells, while OCT provides the relative location information of these tracked cells in the 3D tissue structures. We first proved that the CdS nanowire lasers can be internalized by macrophages and can enhance the OCT signal by up to 25 dB. Then, the distinct lasing emission spectra of nanowire lasers were acquired and used as unique identifiers to track the migration trajectories of cells on fibrin hydrogel surfaces. Finally, we demonstrated the 3D tracking of those nanowire lasers and hence the migration of individual cells in the subretinal layer of living New Zealand rabbits with the dual-modality OCT and FM imaging system.

2. Results

2.1. Experiment setup

In this study, an OCT and FM dual-modality imaging system combined with a spectrometer was developed to monitor the target cells *in vivo* (Fig. 1). In brief, a spectral-domain OCT (SD-OCT) was adapted from a commercially available OCT system. A tunable OPO (optical parametric oscillator) laser with a 1 kHz repetition rate and working at 485 nm was used as the illumination source for lasing emission and FM. The OPO laser light was first collimated by a spatial filter,

Biomedical Optics EXPRESS

and then coaxially combined with the OCT light. Sharing the same galvanometer and telescope configuration, the OPO and OCT laser light was delivered and focused on the same area of interest. The fluorescence and lasing emission were collected through the backward optical path and measured by the photodetector and spectrometer, respectively. The lateral and axial resolution of SD-OCT was previously quantified to be 3.8 μm and 4.0 μm [35,36], respectively, whereas the 2D lateral resolution of FM was 4.0 μm. This system was designed for both *in vitro* cellular studies and *in vivo* animals such as rabbits whose eyes have sizes similar to human eyes. More details about the dual-modality imaging system are described in Material and Methods.

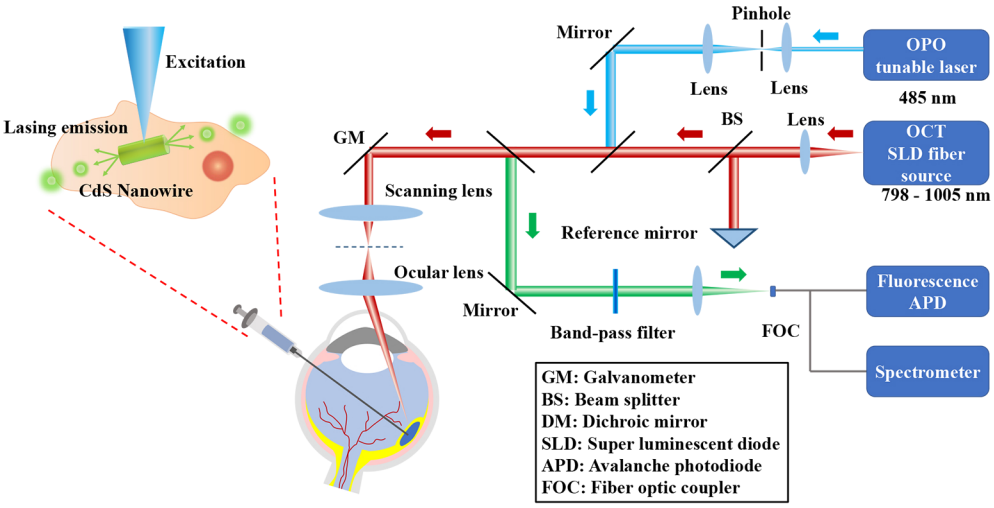

Fig. 1. Schematic of the OCT and fluorescence/laser emission dual-modality imaging system and an illustration of a CdS nanowire microlaser internalized by a cell.

Here we emphasize the role that FM plays in this OCT and FM dual-modality imaging system. First, FM provides cross-validation of cells' spatial locations in OCT images. Second, it helps OCT remove unwanted artifacts. In our data processing, we used OCT signal thresholding to extract the cell positions. Although the OCT signal is strong, some clusters generated by the animal itself exhibit strong scattering and thus appear in the OCT image as artifacts. The 2D information provided by FM about the nanowire locations allows us to easily filter out those artifacts. Third, it assists in laser emission collection. Currently, it takes approximately 2-3 seconds to collect nanowire laser spectrum from one location. It would be very time consuming and impractical to scan the entire tissue. FM helps quickly locate the nanowires within the field of view so that the pump light can be delivered to excite the nanowires, and the corresponding laser emission can subsequently be collected.

2.2. Nanowire laser internalization and characterization

The CdS nanowire lasers were utilized to generate both OCT and FM signal, and unique spectral identifiers to differentiate each individual cell (see more details about nanowire fabrication in the Materials and Methods). Since the CdS nanowire lasers have a small size of 3-7 μm in length and ~200 nm in diameter, they can be easily internalized by macrophages without surface modification. To confirm macrophage nanowire internalization, confocal microscopy was utilized to visualize the 3D cellular structure. In the confocal microscopy image (Fig. 2(a)), the cell cytoskeleton is stained blue and the nuclei are stained red. The CdS nanowire can be visualized by its own green fluorescence under 488 nm laser excitation. From the enlarged top view and side

Biomedical Optics EXPRESS

view images (the top right and the bottom-right insets in Fig. 2(a)) of the selected macrophage, the complete internalization of nanowires within the cell body is confirmed.

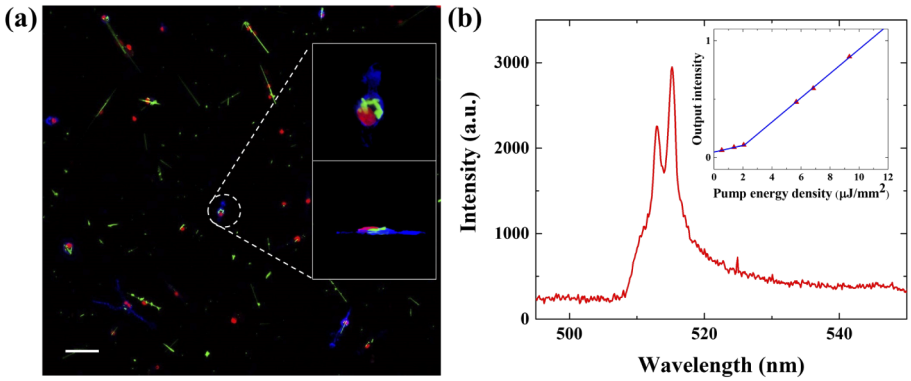

Fig. 2. Nanowire internalized by macrophages and its lasing properties. (a) A confocal fluorescence image of nanowires internalized by macrophages. The cell cytoskeleton is stained blue and the nuclei are stained red. Upper and lower insets are enlarged top view and side view of a specific macrophage, respectively. (b) The lasing spectrum of a nanowire laser. The inset is the threshold curve. Scale bar: 50 μm.

The lasing mechanism of the nanowire lasers can be explained as follows. Due to the high refractive index (n=2.67) of the nanowires, the reflection at its two end-facets is high. Therefore, a nanowire can be regarded as a "Fabry–Perot" (F–P) cavity with a waveguide formed by the gain medium (CdS) and sandwiched between the two end-facets. The Q-factor of the CdS nanowire is estimated to be ~50 [37]. Despite the relatively low Q-factor, CdS can provide a high gain up to ~3000/cm at a carrier density of $1–3\times10^{-19}$ cm^{-3} [38] to compensate for the cavity loss and thus achieve lasing emission at a relatively low excitation. An exemplary lasing emission spectrum of a nanowire laser internalized by macrophage is given in Fig. 2(b). The inset that plots the lasing output vs. pump energy curve shows a lasing threshold of about 2 $\mu J/mm^2$. Meanwhile, due to the high refractive index of CdS (n=2.67) and the elongated shape, the nanowire itself produces strong scattering that can significantly enhance the signal in OCT imaging. Due to the elongated shape of the nanowires, the orientation of the nanowires will influence the signal enhancement. However, no matter which orientation, the OCT signal from the nanowires is much larger than the surrounding tissues. The detailed signal enhancement calibration in OCT is presented in Figs. 7 and 8 in Appendix 1 and 2.

2.3. *In vitro cell tracking with nanowire lasers*

Cell tracking experiments were first conducted *in vitro* to verify feasibility. To mimic the *in vivo* tissue environment, macrophages were cultured on a layer of scattering hydrogel. The sterilized nanowires were added into the cell culture media of macrophages 24 hours before the experiments to ensure full internalization. Then, the macrophages were examined with our dual-modality imaging system. Figures 3(a) and (b) show the fluorescence image and the 2D X-Y plane OCT image from the same area, respectively. The distributions of the macrophages from the two imaging modalities match well, which confirms that the nanowires internalized by the macrophages can provide contrast enhancement in both OCT and FM modalities. The lasing emission spectra were also collected from the nanowire lasers (Fig. 3(c)). Four selected spectra were acquired from the four locations indicated by the yellow boxes in Fig. 3(a) and (b). The distinct lasing emission spectra would be used as an identifier to differentiate each cell for future individual cell tracking.

Biomedical Optics EXPRESS

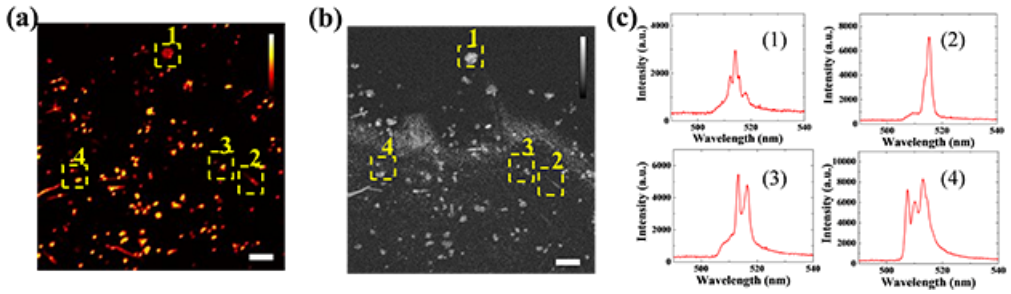

Fig. 3. *In vitro* dual-modality contrast enhancement of nanowire and lasing emission spectra. (a) Fluorescence image of nanowire-labeled macrophages cultured on the hydrogel layer. Four macrophages are selected as tracking targets. (b) 2D X-Y plane OCT image of the same field of view in (a). The locations of the four macrophages labeled with 1-4 match well between (a) and (b). The nanowires provide enhanced imaging contrast in both OCT and FM. (c) Unique lasing spectra (1)-(4) collected from the four selected macrophages in (a) and (b). Scale bar: 100 μm.

After testing the imaging contrast and lasing emission inside the cells, we conducted *in vitro* cell tracking experiments and acquired time-lapse images. Macrophages cultured on fibrin hydrogel were monitored successively every 8 hours for 24 hours in total. During imaging, we used a

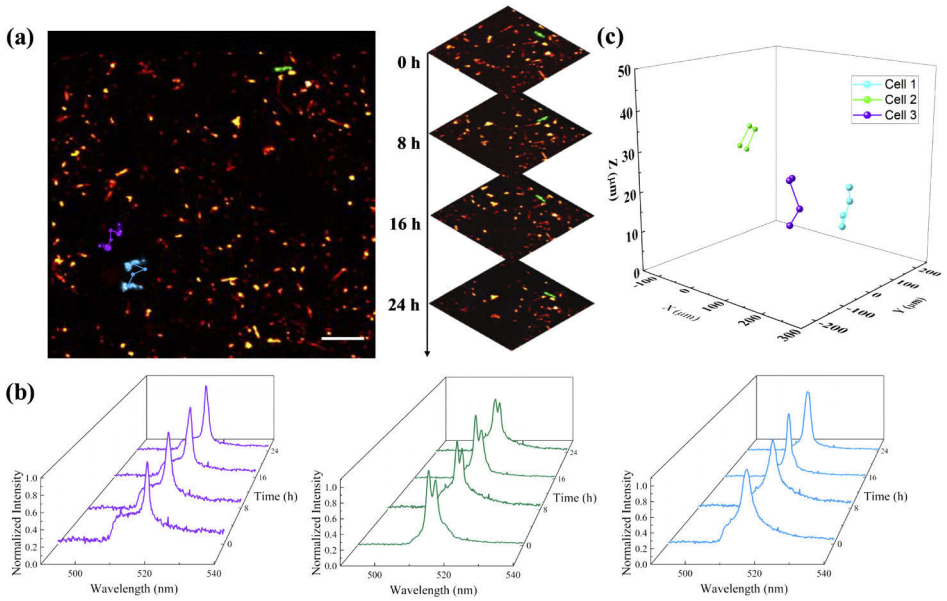

Fig. 4. *In vitro* cell migration tracking. (a) The corresponding fluorescence 2D macrophage migration trajectory. The tracked macrophages are accordingly highlighted with purple, green, and blue. The right inset is a demonstration of macrophage migration over time through multiple frames. (b) The normalized lasing spectra collected for macrophage migration tracking over time. The purple, green, and blue waterfall spectra are corresponding to the same color-labeled macrophages in (a) and (b) respectively. (c) The *in vitro* 3D macrophage migration trajectory extracted from multiple OCT scans over 24 hours. The tracked macrophages are highlighted with purple green and blue. Scale bar: 100 μm.

Biomedical Optics EXPRESS

marker on the fibrin hydrogel surfaces to retrieve the same field of view for each observation. Figure 4(a) shows the migration trajectories of three selected macrophages extracted from the FM images over time. For a clearer view, the trajectories are superimposed on top of each other. The inset on the right shows a series of enlarged views of one macrophage migrating in different time frames. The identities of tracked macrophages are verified by the lasing emission spectra of nanowire laser internalized by the macrophages. Figure 4(b) presents the lasing emission spectra collected from the same selected macrophages in Fig. 4(a). Throughout the entire experiment, the lasing emission spectra from the same macrophages remained unchanged and distinguishable from each other. The OCT 3D images from multiple observations are aligned by matching the structural features of the hydrogel layer. Based on the identification information provided from Fig. 4(b), the individual macrophage spatial location is extracted from the OCT 3D images via contrast thresholding to obtain the migration trajectories of selected macrophages in Fig. 4(c).

2.4. *In vivo* subretinal cell tracking with nanowire lasers

After macrophages internalized nanowires over 24-hour culture, they were re-suspended in a cell-enriched solution. Then, a 20 µL cell-enriched solution was injected into the subretinal layer (Fig. 5(a)) via a Hamilton syringe (see details in Materials and Methods). The *in vivo* cell tracking experiments were conducted 3 days later once the localized subretinal fluid had been absorbed. Figure 5(b) shows a representative cross-sectional image acquired by the OCT of the injection area. The locations of macrophages carrying nanowire lasers are indicated by the red arrows. By analyzing the signal profile along the yellow dashed line in the inset of Fig. 5(b), one can see that the nanowire provides a significant 25 dB OCT signal enhancement compared to the surrounding retinal layers. The OCT X-Y plane projection of the macrophage spatial distribution and the FM image were collected from the same area (Figs. 5(c) and (d), respectively), showing a

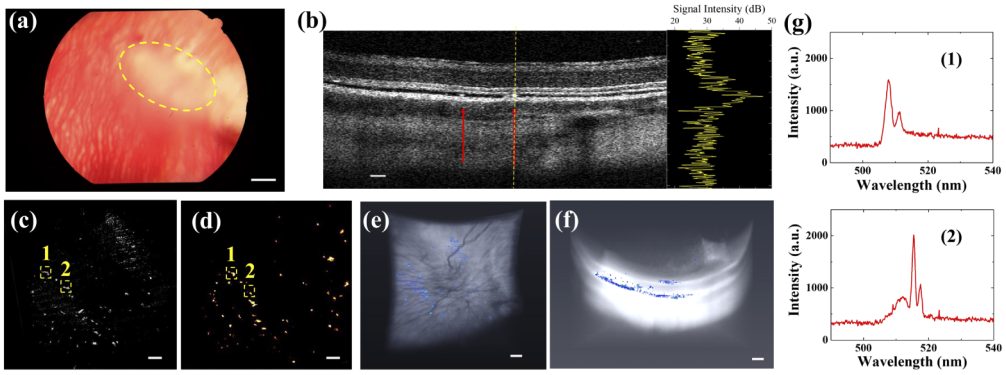

Fig. 5. *In vivo* cell labeling with enhanced OCT and FM dual-modality contrast and lasing emission (a) A color fundus image in albino rabbit. The region of sub-retinal injection of nanowire-labeled macrophages is highlighted. (b) OCT B-scan image collected 2 days after the injection. The nanowire-labeled macrophages are indicated by the red arrows. The right inset is a signal intensity curve collected along the yellow dashed line, which shows that nanowires could provide up to 25 dB signal enhancement compared to the surrounding retinal layers. (c) 2D X-Y plane OCT image of the same field of view in (b) at the same time. (d) FM image of nanowire-labeled macrophages attached to the retinal layer that was acquired from the same field of view in (c). Two of macrophages labeled with nanowires are tracked as (1) and (2). (e)-(f) Top and side views of 3D OCT retinal layer reconstruction and the distribution of macrophages. The nanowire-labeled macrophages are extracted by thresholding segmentation and colored with blue. (g) Two unique lasing spectra (1)-(2) collected from the two tracked macrophages in (e) and (f). Scale bar: 100 µm.

Biomedical Optics EXPRESS

perfect match. Based on this signal enhancement, the 3D total distribution of macrophages in the subretinal layer was extracted by signal thresholding. Figure 5(e) and (f) show the top and side views of 3D OCT image reconstruction, respectively. The retina structure appears as a white region and the macrophage distribution is labeled in blue. Since signal thresholding is utilized to extract the macrophages labeled with nanowire lasers, it will inevitably introduce some noise coming from the retinal structure. Therefore, the density in Fig. 5(e) seems higher than that in Fig. 5(d). By comparing the images from two modalities, only the bright dots shown in both FM and OCT are considered as macrophages. Most of the macrophages were attached under the retina layer, whereas some of them were on the retinal surface due to leakage during the subretinal injection. A 3D rendering video of the retina structure and macrophage distribution is presented in Visualization 1 in the Supplementary Information. Figure 5(g) shows the two selected lasing emission spectra collected from the locations indicated in Fig. 5(c) and (d) to prove that the distinct lasing spectra can be acquired even under the retina layer of living rabbits.

After the localized subretinal fluid was absorbed, macrophage migration was monitored longitudinally for three days. A series of FM images of the area of interest were collected (Fig. 6(a)). For illustration purposes, three macrophages, which are highlighted in green, blue, and purple, respectively, are selected and their lasing spectra are monitored. Figure 6(b) and (c) show the side and top views of 3D OCT image retinal structure reconstruction with the three macrophages, respectively. The retina structure is exhibited in white and the spatial locations of selected macrophages over 3 days are highlighted with the corresponding color. A 3D rendering video of the retina structure and selected macrophage spatial locations are presented in Visualization 2 in the Supplementary Information. It can be seen clearly in Fig. 6(d) that the lasing spectra remained unchanged during the three days of experiment and, therefore, could be

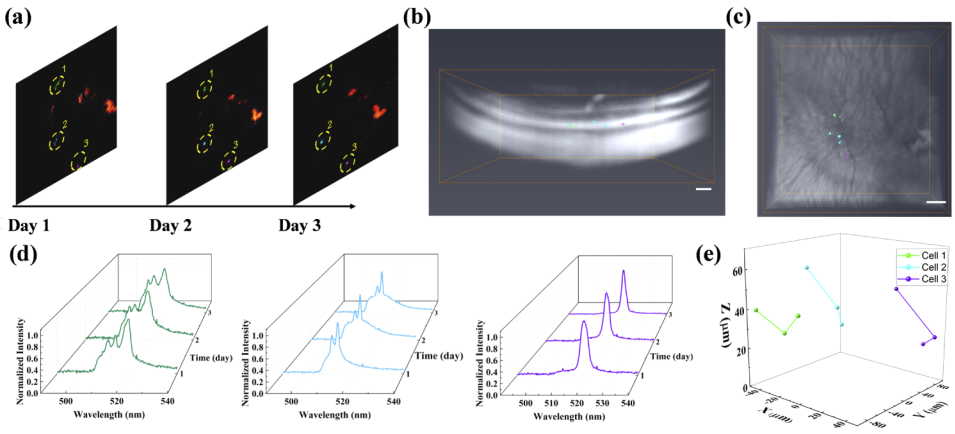

Fig. 6. *In vivo* cell migration tracking. (a) *In vivo* fluorescence images of macrophage migration projections through multiple observations. Three of the tracked macrophages are highlighted with green, blue, and purple. (b)-(c) Side and top views of 3D OCT retinal layer reconstruction and the spatial locations of macrophages. The spatial locations of the same nanowire-labeled macrophages in (a) over 3 days are extracted by thresholding segmentation and superimposed with the retinal structure. The three macrophages are shown with the corresponding colors in (a). (d) Normalized lasing spectra collected for macrophage migration tracking over time. The green, blue, and purple waterfall spectra are corresponding to the same color-labeled macrophages in (a), (b), and (c). (e) The *in vivo* 3D macrophage migration trajectory extracted from multiple OCT scans over 3 days. The tracked macrophages are highlighted with green, blue, and purple accordingly. Scale bar: 100 μm.

Biomedical Optics EXPRESS

used as a unique identifier to distinguish among those three macrophages. In our study, not only the peak wavelengths but the overall lasing pattern was applied to verify the identity of the cells. Even though the absolute peak wavelengths may change due to the change in the surrounding medium, the overall lasing pattern should be consistent and highly correlated over time. Hence, the macrophages can still be recognized by comparing it with the original lasing spectra. With the identity of macrophages verified, the 3D cell migration trajectories are extracted and presented in Fig. 6(e), thus demonstrating the feasibility of *in vivo* single-cell migration tracking with the dual-modality imaging system and nanowire lasers. Here the cell trajectory is based on image coordinates. And the depth is based on the distance between the RPE (retinal pigment epithelium) layer and the center of the macrophages.

3. Conclusions and discussions

In this study, we demonstrated CdS nanowire lasers internalized by macrophages could be utilized as *in vivo* cell tracking identifiers while offering enhanced contrast for both OCT and FM. To validate the feasibility for cell tracking, we first performed *in vitro* experiments to monitor macrophages migration on fibrin hydrogels for 24 hours, and then performed an *in vivo* study to track the macrophages delivered to rabbit eyes via subretinal injection. The injected macrophages were monitored longitudinally *in vivo* for 3 successive days, and the 3D migration trajectories of individual cells were successfully extracted from OCT images.

Our technology, by leveraging the advantages of OCT and lasing emission labeling, provides a new solution for *in vivo* cell tracking. Compared to conventional fluorescence labeling, the lasing emission labeling takes advantage of lasing spectral information such as lasing peaks' positions and relative intensities, rather than merely emission intensity, which provides unique identifications to track the migration of individual cells. Meanwhile, the enhanced OCT contrast by nanowires could provide precise 3D spatial locations of the tracked cells together with 3D tissue structural information. Hence, by integrating the two imaging modalities, *in vivo* tracking of individual cells with high 3D resolution can be achieved in complicated tissue structures such as rabbit eyes as demonstrated in this work.

Compared with other dual-modality imaging systems such as photoacoustic-OCT, our technology could provide spectral identification information from the nanolasers used for cell tracking, while the photoacoustic-OCT imaging system could provide high contrast but homogenous molecular information. In our system, the estimated imaging depth for FM and collection of laser emission spectra is 400 μm, and the imaging depth for OCT is 700 μm. Given the retina has a thickness in humans of 150 to 300 μm and the choroid has a thickness of around 150 μm [39], both are sufficient to track the cells over the entire retinal and choroidal layers in the rabbit eyes. Other deep tissue imaging methods such as two-photon microscopy can also provide high signal-to-noise ratio and high spatial resolution. However, OCT in our dual-modality system offers a deeper imaging depth and, more importantly, is clinically approved for eye imaging and readily used in clinical practice, while the lasing spectra could provide unique identity information at the same time.

For the next step, we plan to change the material of nanowires from low toxicity material CdS to non-toxicity material such as GaN to avoid potential biotoxicological response. In addition, the theoretical number of distinct spectral labels provided by CdS nanowire lasers is approximately 1300, as shown in detail in Section 4.7. The microfabrication design of the nanowire lasers can be improved to provide richer spectral information to label a larger number of cells. Using the current imaging system, the experiments were conducted to acquire an FM image first and then identify the approximate positions of nanowires to collect laser emission spectra, which is time-consuming. In the following study, the dual-modality imaging system will be upgraded to connect the spectrometer with a fluorescence photodetector so that it can simultaneously acquire an FM image and lasing spectra so as to improve the imaging speed. In addition, a spectrometer

Biomedical Optics EXPRESS

with improved spectral resolution will be integrated to better differentiate lasing peaks that are currently difficult to resolve.

Our technique may shed new light on cell-based therapies and understanding of disease models at a single-cell level. For stem cell therapy, this technique may track the migration of stem cells to evaluate treatment efficacy and safety. For research on the role of inflammatory cells in pathologic conditions such as diabetes, macrophages can be tracked when they pass through the retinal layer. Our technology could also be applied to *in vitro* cell tracking studies that require deep imaging depth, such as the studies on organoids and artificial tissues.

4. Material and methods

4.1. Dual-modality imaging system

A schematic of the dual-modality imaging system with integrated SD-OCT, FM, and laser emission is shown in Fig. 1. The system was developed based on an OCT and FM dual-modality imaging system established previously, as described in our previous papers [35,36]. Briefly, the SD-OCT system was adapted from a commercially available system from Thorlabs (Ganymede-II-HR, Thorlabs, Newton, NJ) by implementing an ocular lens (OL) after the scan lens. The ocular lens used was AC080-010-A (Thorlabs, Newton, NJ). For FM and laser excitation, an OPO (NT-242, Ekspla, Vilnius, Lithuania, tunable wavelength from 405 to 2600 nm, pulse duration 3–6 ns) was used as the illumination source. The fluorescence and laser emission were collected from the backward optical path of telescope configuration, reflected by a dichroic mirror (FF496-SDI01, Semrock, Lake Forest, IL) and separated by a fiber optic coupler (TN532R2F1, Thorlabs, Newton, NJ) after passing through a band-pass filter (MF 530-43, CWL = 530 nm, BW = 43 nm, Thorlabs, Newton, NJ) into fluorescence and laser emission channels. The fluorescence signal was detected by an avalanche photodiode (APD) (APD 110A, Thorlabs, Newton, NJ) and digitized by the DAQ card (PX1500–4, Signatec Inc, Newport Beach, CA, sampling rate 500 MHz). The laser emission spectra were collected by the spectrometer with an integration time of 0.5 s (HR4000, Ocean Optics Inc, Dunedin, FL). The OPO laser, the OCT scan header, and the DAQ card were synchronized through a delay generator and a clock switch circuit. The light beams from different imaging modalities were coaxially aligned to ensure the co-registration of the dual-modality images. The lateral and axial resolution of SD-OCT were previously quantified to be 3.8 μm and 4.0 μm, respectively [35,40]. In this study, the laser wavelength of 485 nm and the laser energy of 150 nJ before the eye were used.

4.2. Nanowire lasers preparation

The method of synthesizing CdS nanowires was described in detail in the previous publications [30,37,41]. Briefly, the nanowires were synthesized by an Au-nanocluster catalyzed vapor-liquid-solid method. Inside a horizontal quartz tube mounted in a single zone furnace, CdS powders (Sigma Aldrich, St. Louis, MO, 99.99% purity) were placed on an alumina boat in the center of the heating zone as the source. Silicon (Si) wafers (Ql Electronics Inc., Ningbo, China) covered with a 10 nm thick Au film by sputtering were located downstream from CdS powders near the end of the heating zone. A high purity nitrogen gas flow with a flow rate of 700 SCCM was introduced into the system to purge oxygen out. After 1 hour of gas flow cleaning, the furnace was heated from room temperature to 850 °C at 500 mbar pressure and kept for an extra hour. Meanwhile, a 155 SCCM nitrogen gas flow was maintained in the whole heating process to transport the evaporated CdS vapor to the Au-catalyzed Si substrates to initialize nanowire growth. After growing for 1 hour, yellowish nanowire products could be found on the Si substrate.

Biomedical Optics EXPRESS

4.3. Cell preparation

The isolation of bone morrow-derived macrophages was conducted as the previously described [42]. Mice were first sacrificed by cervical dislocation. Then, the abdomen and hind legs were sterilized with 70% ethanol. After making an incision in the midline of the abdomen, the hind legs were exposed, and the bones were cut at both ends. Later on, the bones were crushed in a mortar with 5 mL of lymphocyte medium supplemented with 20 mM HEPES. The bone marrow cells were pipetted up and down to separate the cells into single-cell suspension for them to pass through a cell strainer. The cells were transferred into bone morrow macrophage medium and induced to differentiate in a humidified incubator with 5% CO_2 at 37 °C. Macrophage media consisted of DMEM containing 1% penicillin/streptomycin, L-glutamine, 10% fetal bovine serum, and L929 murine fibroblast conditioned media (All supplies were from Thermo Fisher, Waltham, MA).

4.4. In vitro experiments

For biological use, the nanowire-carrying wafer was immersed in ethanol and sonicated in an ultrasonic cleaner for 10 min to separate the nanowires from the substrate. After removal of the Si substrate and centrifuging of the remaining solution, the nanowires were separated from ethanol, then re-dispersed in phosphate-buffered saline (PBS) solution, and finally sterilized under a UV lamp for about 1 hour in a laminar flow hood before culturing with the cells.

To mimic the *in vivo* subretinal layer environment, macrophages were seeded on a layer of fibrin hydrogel. Fibrin hydrogel coated glass coverslips were made by adding 100 µl of fibrin precursor solution (5 mg/ml fibrinogen (Sigma Aldrich, St. Louis, MO) and 10 units/ml thrombin (Sigma Aldrich) in 1X PBS) onto 18 mm diameter glass coverslips and allowed to crosslink for 30 minutes. The nanowire-carrying macrophages were then seeded onto 5 mg/ml fibrin hydrogel coated coverslips and allowed to attach and spread over 24 hours. Next, 150 µL PBS solution of containing nanowires was added overlying cell media (2 mL), and cells were allowed to internalize nanowires over 24 hours. Then samples were rinsed with media 3x to ensure that free-floating nanowires were removed prior to longitudinal imaging. The cell viability after internalizing nanowire lasers was verified in our previous paper [30].

The rate of success for internalization is around 70%. The internalization is currently ensured by adding a higher concentration of nanowire solutions, rinsing multiple times, and conducting rigorous shaking during the cell preparation steps before injection. To verify that the nanowires were internalized by macrophages, confocal images were acquired on a confocal microscope (LSM800, Zeiss, Jena, Germany). Samples were first fixed with 4% paraformaldehyde. Then 4′,6-diamidino-2-phenylindole (DAPI) (1 µg/ml, Sigma Aldrich, St. Louis, MO) and Phalloidin 555 (Life Technologies, Carlsbad, CA) were used to visualize cell nuclei and F-actin, respectively.

4.5. Animal preparation

All animals procedures adhered to the ARVO (The Association for Research in Vision and Ophthalmology) Statement for the Use of Animals in Ophthalmic and Vision Research and were approved by the Institutional Animal Care & Use Committee (IACUC) of the University of Michigan (Protocol PRO00008566, Photoacoustic & Molecular Imaging of the Eye, PI: Y. Paulus).

Five New Zealand white rabbits (both genders, 3-4 months old, 1.5-2.5 kg) were involved in this study. Rabbits were anesthetized with a mixture of Ketamine (40 mg/kg) and Xylazine (5 mg/kg) by intramuscular injection. A vaporized isoflurane anesthetic (1 L/min oxygen and 0.75% isoflurane) (SurgiVet, MN, USA) maintained anesthesia during the *in vivo* experiments. Pupillary dilation was achieved by one drop each of 1% tropicamide and 2.5% phenylephrine hydrochloride. Topical tetracaine 0.5% was instilled before treatment for topical anesthesia. Rabbit vital signs were monitored before and throughout the procedures, including mucous

Biomedical Optics EXPRESS

membrane color, temperature, heart rate, respiratory rate, and oxygen saturation using a pulse oximeter (V8400D Capnograph & SpO2 Digital Pulse Oximetry, Smiths Medical, MN, USA).

4.6. In vivo experiments

To prepare for the subretinal injection, macrophages cultured with nanowires were collected by adding Accutase for 10 min at room temperature and enriched by centrifuging at 500 RCF for 4 min. The subretinal injection was performed via a sterile technique. The conjunctiva was cleaned with 5% povidone-iodine. A 3-mm inferotemporal conjunctival peritomy was performed in the eye using Westcott scissors and micro-forceps. After a marker was used to measure a distance 3.5 mm posterior to the corneal limbus, a 30-gauge 0.5-inch needle was inserted at about the 8:00 to 8:30 position with care to avoid the ciliary vasculature and extraocular muscles. The OCT system was used for real-time guidance and assisting in confirming the injection depth by providing the anatomy of the injected retinal layers at 11 frames per second. A blunt 30-gauge needle (Hamilton, Reno, NV) attached to a 50 µL Hamilton syringe (Hamilton, Reno, NV) was inserted through the 30-gauge 0.5-inch needle inserted site into the vitreous cavity, then introduced into the subretinal space about 0.5–1 optic disc diameter inferior to the retinal vessels, to inject 20µL of macrophage-enriched solution. When the needle was in contact with the RPE (retinal pigment epithelium) hyper-reflective layer, it was stopped and maintained its position before the syringe was pushed. The injection resulted in a localized subretinal fluid. During experiments, eyewash (Altaire Pharmaceuticals, Inc., Aquebogue, NY) was applied to the rabbit corneal surface every 2 min to prevent corneal surface keratopathy. The rabbit fundus was first imaged using a fundus camera (TRC 50EX, Topcon Corporation, Tokyo, Japan). After finishing the fundus camera imaging, the rabbits were transferred to the platform of the dual-modality imaging system and adjusted to position one eye under the ophthalmic lens. The head and body of the rabbit were placed on two custom-made stabilization platforms, which were used to minimize breathing and other motion artifacts. A water-circulation blanket (TP-700, Stryker Corporation, Kalamazoo, MI) was used to maintain the body temperature of the rabbits. The eyelid was retracted with a pediatric Barraquer wire speculum. The integrated charge-coupled device (CCD) camera was used to visualize the region of interest, and the reference arm was adjusted to optimize the image quality. During the experiments, the 3D OCT scanning was conducted first. Then, a 2D FM image was collected. Based on the FM images, an algorithm of contour detection and weighted center calculation was used to identify the locations of nanowires internalized by the macrophages and control the OPO laser beam to re-visit those locations to excite nanowire laser emission and collect corresponding lasing spectra. In addition, to visualize the distribution of nanowire-labeled macrophages and subretinal structures, 3D image reconstruction and processing were performed using the Amira software (FEI, Hillsboro, OR).

4.7. Calculation of the number of labels

The calculation of potential unique spectral labels from the CdS nanowire lasers. The lasing emission peaks range from 500 nm to 525 nm. Given our current spectrometer resolution of ~1 nm, the number of distinct spectral labels with 1 peak is:

$$N_1 = \begin{pmatrix} 20 \\ 1 \end{pmatrix} = 20$$

Since there are also spectral labels with 2 lasing peaks, the number of potential distinct spectral labels are:

$$N_2 = \begin{pmatrix} 20 \\ 2 \end{pmatrix} = 190$$

Biomedical Optics EXPRESS

Similarly, the number of spectral labels with 3 peaks is:

$$N_3 = \begin{pmatrix} 20 \\ 3 \end{pmatrix} = 1140$$

Because the spectral labels with 4 peaks rarely occur, the total number can be calculated as:

$$N_{total} = N_1 + N_2 + N_3 = 1350$$

Appendix 1

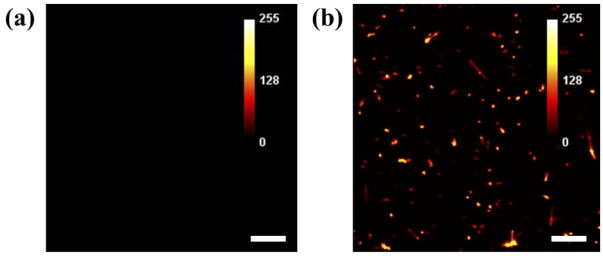

Fig. 7. Fluorescence contrast from CdS nanowire lasers. (a) An FM image of macrophages without Cd nanowire lasers. (b) An FM image of macrophages with CdS nanowire lasers. Scale bar: 100 μm.

Appendix 2

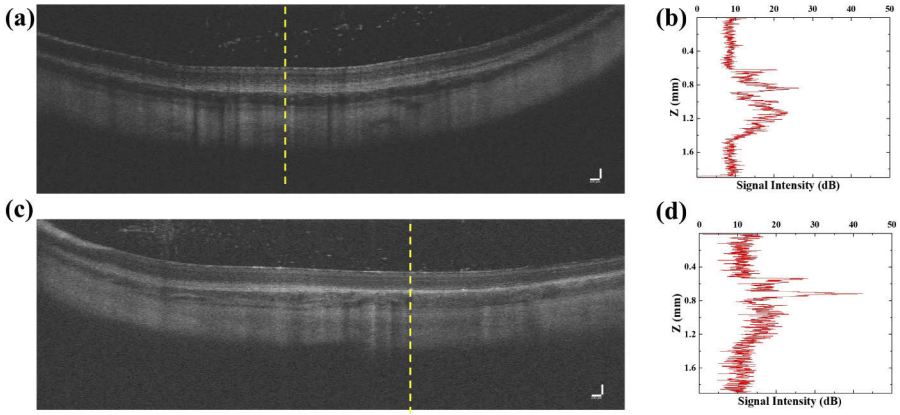

Fig. 8. OCT contrast from CdS nanowire lasers. (a) An OCT cross-sectional image of macrophages without Cd nanowire lasers. (b) An imaging contrast profile measured along the yellow dashed line in (a). (c) An OCT cross-sectional image of macrophages in the subretinal layer with CdS nanowire lasers. (d) An imaging contrast profile measured along the yellow dashed line in (c). Scale bar: 100 μm.

Funding

National Science Foundation (ECCS-1607250); National Institutes of Health (1K08EY027458, R01EY029489).

Biomedical Optics EXPRESS

Acknowledgments

The authors would like to thank Dr. Yuqing Eugene Chen and the Center for Advanced Models for Translational Sciences and Therapeutics (CAMTraST) at the University of Michigan Medical School for the generous donation of New Zealand white rabbits.

Disclosures

[+]Xuzhou Li and Wei Zhang contributed equally to this work.

The authors declare that there are no conflicts of interest related to this article.

References

1. A. Trounson, R. G. Thakar, G. Lomax, and D. Gibbons, "Clinical trials for stem cell therapies," BMC Med. **9**(1), 52 (2011).
2. J. Kang, S. Demaria, and S. Formenti, "Current clinical trials testing the combination of immunotherapy with radiotherapy," J. Immunother. Cancer **4**(1), 51 (2016).
3. J. Tang, D. Shen, T. G. Caranasos, Z. Wang, A. C. Vandergriff, T. A. Allen, M. T. Hensley, P.-U. Dinh, J. Cores, and T.-S. Li, "Therapeutic microparticles functionalized with biomimetic cardiac stem cell membranes and secretome," Nat. Commun. **8**(1), 1–9 (2017).
4. R. Sharma, V. Khristov, A. Rising, B. S. Jha, R. Dejene, N. Hotaling, Y. Li, J. Stoddard, C. Stankewicz, and Q. Wan, "Clinical-grade stem cell–derived retinal pigment epithelium patch rescues retinal degeneration in rodents and pigs," Sci. Transl. Med. **11**(475), eaat5580 (2019).
5. L. Wang, L. Wang, X. Cong, G. Liu, J. Zhou, B. Bai, Y. Li, W. Bai, M. Li, and H. Ji, "Human umbilical cord mesenchymal stem cell therapy for patients with active rheumatoid arthritis: safety and efficacy," Stem Cells Dev. **22**(24), 3192–3202 (2013).
6. J. Panés, D. García-Olmo, G. Van Assche, J. F. Colombel, W. Reinisch, D. C. Baumgart, A. Dignass, M. Nachury, M. Ferrante, and L. Kazemi-Shirazi, "Long-term efficacy and safety of stem cell therapy (Cx601) for complex perianal fistulas in patients with Crohn's disease," Gastroenterology **154**(5), 1334–1342.e4 (2018).
7. M. F. Kircher, S. S. Gambhir, and J. Grimm, "Noninvasive cell-tracking methods," Nat. Rev. Clin. Oncol. **8**(11), 677–688 (2011).
8. D. Huang, E. A. Swanson, C. P. Lin, J. S. Schuman, W. G. Stinson, W. Chang, M. R. Hee, T. Flotte, K. Gregory, and C. A. Puliafito, "Optical coherence tomography," Science **254**(5035), 1178–1181 (1991).
9. C. A. Puliafito, M. R. Hee, C. P. Lin, E. Reichel, J. S. Schuman, J. S. Duker, J. A. Izatt, E. A. Swanson, and J. G. Fujimoto, "Imaging of macular diseases with optical coherence tomography," Ophthalmology **102**(2), 217–229 (1995).
10. W. Drexler, U. Morgner, F. X. Kartner, C. Pitris, S. A. Boppart, X. D. Li, E. P. Ippen, and J. G. Fujimoto, "In vivo ultrahigh-resolution optical coherence tomography," Opt. Lett. **24**(17), 1221–1223 (1999).
11. X. Yao, K. Devarajan, R. M. Werkmeister, V. A. dos Santos, M. Ang, A. Kuo, D. W. Wong, J. Chua, B. Tan, and V. A. Barathi, "In vivo corneal endothelium imaging using ultrahigh resolution OCT," Biomed. Opt. Express **10**(11), 5675–5686 (2019).
12. K. Li, W. Liang, Z. Yang, Y. Liang, and S. Wan, "Robust, accurate depth-resolved attenuation characterization in optical coherence tomography," Biomed. Opt. Express **11**(2), 672–687 (2020).
13. S. A. Boppart, B. E. Bouma, C. Pitris, J. F. Southern, M. E. Brezinski, and J. G. Fujimoto, "In vivo cellular optical coherence tomography imaging," Nat. Med. **4**(7), 861–865 (1998).
14. E. J. Fernandez, B. Hermann, B. Povazay, A. Unterhuber, H. Sattmann, B. Hofer, P. K. Ahnelt, and W. Drexler, "Ultrahigh resolution optical coherence tomography and pancorrection for cellular imaging of the living human retina," Opt. Express **16**(15), 11083–11094 (2008).
15. S. M. Rey, B. Povazay, B. Hofer, A. Unterhuber, B. Hermann, A. Harwood, and W. Drexler, "Three- and four-dimensional visualization of cell migration using optical coherence tomography," J. Biophotonics **2**(6-7), 370–379 (2009).
16. T. M. Lee, A. L. Oldenburg, S. Sitafalwalla, D. L. Marks, W. Luo, F. J. Toublan, K. S. Suslick, and S. A. Boppart, "Engineered microsphere contrast agents for optical coherence tomography," Opt. Lett. **28**(17), 1546–1548 (2003).
17. A. Agrawal, S. Huang, A. Wei Haw Lin, M. H. Lee, J. K. Barton, R. A. Drezek, and T. J. Pfefer, "Quantitative evaluation of optical coherence tomography signal enhancement with gold nanoshells," J. Biomed. Opt. **11**(4), 041121 (2006).
18. T. S. Troutman, J. K. Barton, and M. Romanowski, "Optical coherence tomography with plasmon resonant nanorods of gold," Opt. Lett. **32**(11), 1438–1440 (2007).
19. Y. Ponce de León, J. L. Pichardo-Molina, N. Alcalá Ochoa, and D. Luna-Moreno, "Contrast enhancement of optical coherence tomography images using branched gold nanoparticles," J. Nanomater. **2012**, 1–9 (2012).
20. A. Gao, W. Xu, Y. Ponce de Leon, Y. Bai, M. Gong, K. Xie, B. H. Park, and Y. Yin, "Controllable Fabrication of Au Nanocups by Confined-Space Thermal Dewetting for OCT Imaging," Adv. Mater. **29**, 1701070 (2017).

Biomedical Optics EXPRESS

21. K. M. Au, Z. Lu, S. J. Matcher, and S. P. Armes, "Polypyrrole nanoparticles: a potential optical coherence tomography contrast agent for cancer imaging," Adv. Mater. **23**(48), 5792–5795 (2011).
22. K. Kurokawa, Z. Liu, J. Crowell, F. Zhang, and D. T. Miller, "Method to investigate temporal dynamics of ganglion and other retinal cells in the living human eye," Proc. SPIE **10474**, 104740W (2018).
23. E. B. Voura, J. K. Jaiswal, H. Mattoussi, and S. M. Simon, "Tracking metastatic tumor cell extravasation with quantum dot nanocrystals and fluorescence emission-scanning microscopy," Nat. Med. **10**(9), 993–998 (2004).
24. C. Lin, R. Jungmann, A. M. Leifer, C. Li, D. Levner, G. M. Church, W. M. Shih, and P. Yin, "Submicrometre geometrically encoded fluorescent barcodes self-assembled from DNA," Nat. Chem. **4**(10), 832–839 (2012).
25. C. T. Kuo, H. S. Peng, Y. Rong, J. Yu, W. Sun, B. Fujimoto, and D. T. Chiu, "Optically Encoded Semiconducting Polymer Dots with Single-Wavelength Excitation for Barcoding and Tracking of Single Cells," Anal. Chem. **89**(11), 6232–6238 (2017).
26. W. Li, W. Song, B. Chen, and S. J. Matcher, "Superparamagnetic graphene quantum dot as a dual-modality contrast agent for confocal fluorescence microscopy and magnetomotive optical coherence tomography," J. Biophotonics **12**(2), e201800219 (2019).
27. M. Humar and S. H. Yun, "Intracellular microlasers," Nat. Photonics **9**(9), 572–576 (2015).
28. M. Schubert, A. Steude, P. Liehm, N. M. Kronenberg, M. Karl, E. C. Campbell, S. J. Powis, and M. C. Gather, "Lasing within live cells containing intracellular optical microresonators for barcode-type cell tagging and tracking," Nano Lett. **15**(8), 5647–5652 (2015).
29. A. H. Fikouras, M. Schubert, M. Karl, J. D. Kumar, S. J. Powis, A. Di Falco, and M. C. Gather, "Non-obstructive intracellular nanolasers," Nat. Commun. **9**(1), 4817 (2018).
30. X. Wu, Q. Chen, P. Xu, Y. C. Chen, B. Wu, R. M. Coleman, L. Tong, and X. Fan, "Nanowire lasers as intracellular probes," Nanoscale **10**(20), 9729–9735 (2018).
31. Z. Lv, Z. Man, Z. Xu, C. Feng, Y. Yang, Q. Liao, X. Wang, L. Zheng, and H. Fu, "Intracellular near-infrared microlaser probes based on organic microsphere-SiO_2 core-shell structures for cell tagging and tracking," ACS Appl. Mater. Interfaces **10**(39), 32981–32987 (2018).
32. N. Martino, S. J. J. Kwok, A. C. Liapis, S. Forward, H. Jang, H.-M. Kim, S. J. Wu, J. Wu, P. H. Dannenberg, S.-J. Jang, Y.-H. Lee, and S.-H. Yun, "Wavelength-encoded laser particles for massively multiplexed cell tagging," Nat. Photonics **13**(10), 720–727 (2019).
33. M. Schubert, L. Woolfson, I. R. Barnard, A. Morton, B. Casement, G. B. Robertson, G. B. Miles, S. J. Pitt, C. S. Tucker, and M. C. Gather, "Monitoring contractility in single cardiomyocytes and whole hearts with bio-integrated microlasers," bioRxiv **2019**, 605444 (2019).
34. X. Li, Y. Qin, X. Tan, Y.-C. Chen, Q. Chen, W.-H. Weng, X. Wang, and X. Fan, "Ultrasound modulated droplet lasers," ACS Photonics **6**(2), 531–537 (2019).
35. C. Tian, W. Zhang, V. P. Nguyen, X. Wang, and Y. M. Paulus, "Novel photoacoustic microscopy and optical coherence tomography dual-modality chorioretinal imaging in living rabbit eyes," J. Visualized Exp. **8**(132), e57135 (2018).
36. W. Zhang, Y. Li, V. P. Nguyen, Z. Huang, Z. Liu, X. Wang, and Y. M. Paulus, "High-resolution, in vivo multimodal photoacoustic microscopy, optical coherence tomography, and fluorescence microscopy imaging of rabbit retinal neovascularization," Light: Sci. Appl. **7**(1), 103 (2018).
37. X. Wu, Q. Chen, P. Xu, L. Tong, and X. Fan, "Refractive index sensing based on semiconductor nanowire lasers," Appl. Phys. Lett. **111**(3), 031112 (2017).
38. A. V. Maslov and C. Z. Ning, "Modal gain in a semiconductor nanowire laser with anisotropic bandstructure," IEEE J. Quantum Electron. **40**(10), 1389–1397 (2004).
39. H. Kolb, E. Fernandez, and R. Nelson, *Bipolar Cell Pathways in the Vertebrate Retina–Webvision: The Organization of the Retina and Visual System* (University of Utah Health Sciences Center, 1995).
40. C. Tian, W. Zhang, A. Mordovanakis, X. Wang, and Y. M. Paulus, "Noninvasive chorioretinal imaging in living rabbits using integrated photoacoustic microscopy and optical coherence tomography," Opt. Express **25**(14), 15947–15955 (2017).
41. C. Ma and Z. L. Wang, "Road map for the controlled synthesis of CdSe nanowires, nanobelts, and nanosaws—a step towards nanomanufacturing," Adv. Mater. **17**(21), 2635–2639 (2005).
42. J. Weischenfeldt and B. Porse, "Bone marrow-derived macrophages (BMM): isolation and applications," Cold Spring Harb. Protoc. **2008**(12), pdb.prot5080 (2008).